Since January 2020 Elsevier has created a COVID-19 resource centre with free information in English and Mandarin on the novel coronavirus COVID-19. The COVID-19 resource centre is hosted on Elsevier Connect, the company's public news and information website.

Available online at www.sciencedirect.com
ScienceDirect
Building and Environment 44 (2009) 44–55
BUILDING AND ENVIRONMENT
www.elsevier.com/locate/buildenv

Transport of exhaled particulate matter in airborne infection isolation rooms

Jennifer Richmond-Bryant*

Environmental and Occupational Health Sciences, Hunter College, City University of New York, 425 East 25th Street, New York City, NY 10010, USA

Received 30 July 2007; received in revised form 22 January 2008; accepted 23 January 2008

Abstract

The goal of this research was to examine the characteristics of the spatial velocity and concentration profiles which might result in health care workers' exposure to a pathogenic agent in an airborne infection isolation room (AIIR). Computational fluid dynamics simulations were performed for this purpose. This investigation expanded on the work of Huang and Tsao [The influence of air motion on bacteria removal in negative pressure isolation rooms. HVAC & R Research 2005; 11: 563–85], who studied how ventilation conditions impact dispersion of pathogenic nuclei in an AIIR by investigating the airflow conditions impacting dispersion of infectious agents in the AIIR. The work included a careful quality assurance study of the computed airflow, and final simulations were performed on a fine tetrahedral mesh with approximately 1.3×10^6 cells. The 1 μm diameter particles were released from a 0.001225 m^2 area representing the nose and mouth. Two cases were investigated during the current study: continuous exhalation of pathogen-laden air from the patient and expulsion of pathogenic particles by a single cough or sneeze. Slow decay of particle concentration in the AIIR during the single cough/sneeze simulation and tendency for particle accumulation near the AIIR walls observed in the continuous breathing simulation suggest that unintended exposures are possible despite the ventilation system. Based on these findings, it is recommended that extra care be taken to assure proper functionality of personal protective equipment used in an AIIR.

Keywords: Airborne infection isolation room; Aerosol transport; Computational fluid dynamics; Indoor air quality; Particle transport

1. Introduction

A number of administrative and engineering controls are commonly employed to protect health care workers and other hospital patients from exposure to highly infectious airborne pathogens [1,2]. Airborne infection isolation rooms (AIIRs) are designed to protect facility occupants outside the room. A separate ventilation system is used for the AIIR to prevent mixing of potentially contaminated air with fresh intake air for the ventilation system serving the majority of the hospital. The AIIR infiltration and exhaust air supplies maintain negative pressure within the room to prevent the pathogens from entering other parts of the hospital and to minimize concentrations of the pathogen inside the AIIR.

Within the AIIR, administrative controls are typically used for worker protection. These include use of personal protective equipment (PPE) and thorough hand disinfection. Type N_{95} respirators are routinely used to prevent health care workers' exposure to airborne nuclei of infectious bacterial or viral pathogens [3]. Potential for exposure exists when respirators do not fit the employees properly. Face seal leakage can occur under a variety of conditions, such as when fit testing is inadequate, the healthcare worker has gained or lost weight since the most recent fit test, or the healthcare worker is not cleanly shaven when visiting infectious disease patients [4]. Moreover, Yen et al. [1] maintain that, while important, the standard protocols for preventing infectious disease may not be sufficient. Ofner et al. [5] found that health care workers were infected with severe acute respiratory syndrome (SARS) when wearing PPE that was believed to be sufficient. Hence, administrative controls may not be adequate for health care workers entering AIIRs, even if

*Tel.: +1 212 481 7580; fax: +1 212 481 5260.
E-mail address: jrichmon@hunter.cuny.edu

0360-1323/$ - see front matter © 2008 Elsevier Ltd. All rights reserved.
doi:10.1016/j.buildenv.2008.01.009

the AIIR protects occupants of the remainder of the hospital.

Given the concern for lack of protection within an AIIR, it is important to develop an understanding of air and contaminant transport in the room. A comprehensive review of studies of airborne transmission of infectious agents has demonstrated conclusive evidence that air movement can contribute to transmission and subsequent outbreak of infectious disease [6]. Laboratory and computational research has shown that the well-mixed assumption is not necessarily valid immediately after an aerosol is released [7,8]. Instead, non-dimensional aerosol residence time has been shown to be a function of turbulence intensity, which in turn is a function of positioning of the ventilation inlets and outlets and furnishings. In support of that point, transmission of exhaled air from one body to another and resulting airborne concentration have been shown for displacement ventilation and hospital rooms to depend on the position of the source, turbulence caused by movement of mannequins, and turbulence caused by the ventilated air interacting with surfaces and heat plumes in a room [9,10]. Other computational studies have demonstrated a relationship between the aerosol residence time and convective transport [11]. Knowledge of the airflow patterns may thus elucidate concentration gradients. Graded distribution of the pathogen concentration with respect to the patient's breathing zone may facilitate creation of a spatial probability exposure distribution within the room. This, in turn, may guide determination of safe behavior practices within an AIIR.

Given the sensitivity of taking and handling biological aerosol samples in an AIIR, computational fluid dynamics (CFD) analysis techniques are especially appropriate for the problem of highly infectious pathogen particulate transport. CFD can provide a highly resolved estimate of air and species transport within the region of interest in lieu of obtaining field samples, because AIIRs may be difficult to access and samples may be dangerous to obtain and analyze. CFD has been employed to compare ventilation designs in hospital rooms [10] and AIIRs [12–14], study the dispersion of tuberculosis nuclei [15], and assess the effect of human movement on pathogen dispersion in an AIIR [16].

The goal of this analysis was to examine the characteristics of the spatial velocity and concentration profiles, which might lead the health care worker to be exposed to a pathogenic agent in an AIIR. The study expanded on the work of Huang and Tsao [12] which studies the removal of pathogenic nuclei emitted by one patient's breathing and forced expulsion (cough/sneeze) under a variety of ventilation conditions. In addition to the patient, the current study includes a health care worker for the purpose of examining that worker's potential for exposure to the infectious agent. The ventilation design shown in Huang and Tsao [12] to be most successful in removing the pathogenic particles is employed here, and both the healthcare worker and the patient are heated to represent actual conditions.

2. Simulation methods

Indoor air motion is governed by the Navier–Stokes equations for conservation of momentum and by conservation of mass and have been solved using a variety of approximation and closure methods over the past 40 years. They are not provided here because they appear in numerous references [17–19]. For this study, CFD simulations were performed using the Fluent v.6.1.22 software (Fluent, Inc., Lebanon, NH), with mesh generation from the Gambit v.2.3.16 pre-processor. The Fluent software is designed to approximate the Navier–Stokes equations by a selected approximation model and then solve the set of equations for the designated boundary conditions using a finite volume method. A transient simulation was performed for studying the time evolution of nuclei transport. For these simulations, the realizable $k\sim\varepsilon$ method was employed because it has been proven to model separating flows with better accuracy than the standard $k\sim\varepsilon$ method but is not as time-consuming to run as a large eddy simulation [19].

The room geometry, modeled after the geometry used in Huang and Tsao [12], is shown in Fig. 1. The room is 5.5 m wide, 3.6 m deep, and 2.3 m high. The 2.2 m wide, 2.15 m deep, 2.3 m high bathroom within the AIIR was removed from the domain because it was assumed to be treated as a separate zone. The bed containing the patient was centered at $x = 4$ m with the back of the bed against the bottom wall of the AIIR (when looking at Fig. 1). The bed/patient was 1 m wide, 1.9 m deep, and 0.7 m high. The patient's head was an ellipsoid with a 0.001225 m^2 strip across the front to represent the nose and mouth area. This area matched that simulated by Huang and Tsao [12], although they used a cubic representation for the head. Last, the 1.62 m tall health care worker was centered at $x = 3.2$ m, $y = 0.645$ m. This height was selected based on the National Health and Nutrition Examination Survey 50th percentile female height for all ethnicities in the United States [3]. The body geometry of the health care worker approximated human geometry with an ellipsoidal head, rounded shoulders and torso, and straight legs. However, limbs were not modeled. The health care worker geometry is shown in Fig. 2.

Boundary conditions used for the airflow simulation are shown in Table 1. An air exchange rate of 8.66 air changes per hour (ACH) was employed to match the optimized ventilation conditions found by Huang and Tsao [12]. Three types of boundaries were used in the simulation. Boundary conditions for velocity inlets into the room were established for air movement under the door crack, the ventilation inlet, and the patient's mouth. As performed in Huang and Tsao [12], a grille-style inlet was used to produce unidirectional airflow into the room. Following Huang and Tsao [12], no bathroom zone was represented, so a negatively pressurized door crack to the bathroom was not included in this simulation. If a door were located behind the health care worker, classical ventilation work on slot exhaust velocities [20] and more recent CFD work

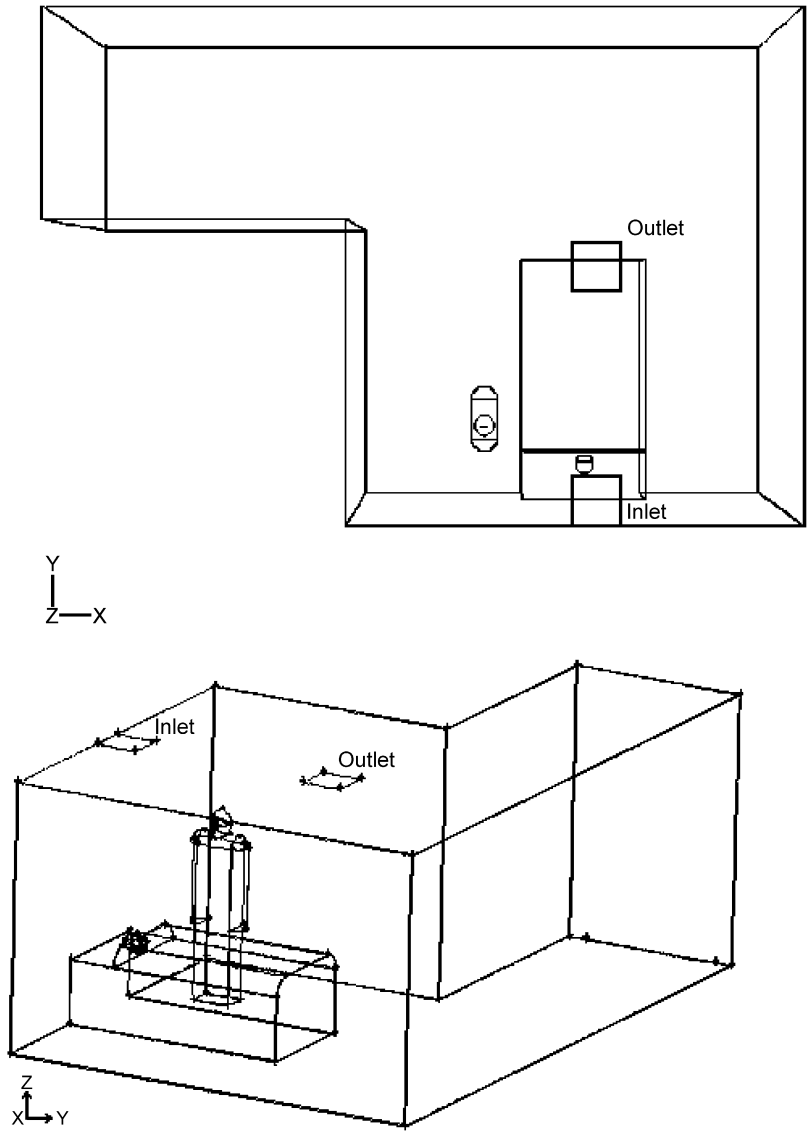

Fig. 1. (Top) Plan view and (bottom) isometric view of the AIIR modeled in the simulations. The AIIR is 5.5 m wide, 3.6 m deep, and 2.3 m high.

on this [21] (assuming that a bathroom would be negatively pressurized) can be consulted to estimate the impact. It would be expected that a door crack of area 0.012 m^2 would exert air movement in the direction of the wall within approximately 0.3 m of the crack at the floor. Given that the primary area of interest in the simulation is the breathing zone area around the health care worker and above the patient, all of which are at least 0.5 m above the zone of interest, the impact of a door crack leading to the bathroom would be expected to be negligible. Wall boundary designations meant that no-slip and no-flow conditions were established for those geometric entities.

Thermal boundary conditions were also included to consider the effect of temperature gradients on air and contaminant motion. The AIIR walls, floor, and ceilings all had wall designations set to a temperature of 297.15 K except for the outer wall, which is set at 303.15 K. The bed, patient's body, health care worker's body, and health care worker's head were also designated as wall boundaries. The temperatures used in Huang and Tsao [12] were replicated for the ventilation units, patient head, and bed. For the health care worker, the body temperature was 307.75 K to reflect the insulation properties of clothing, and the head was set to 308.75 K for normal body temperature.

Simulations were performed on three successively finer tetrahedral meshes with $36 \times 36 \times 16$, $72 \times 72 \times 32$, and $144 \times 144 \times 64$ elements. The grid convergence index was used to determine the error resulting from mesh size [22]:

$$\mathrm{GCI} = F_s \frac{\varepsilon}{r^p - 1}, \tag{1}$$

where F_s is a factor of safety, ε is the relative L_2 error norm of the velocity magnitude, r is the mesh refinement ratio, and p is the order of the method. In this study, F_s was designated to be 1.25 here because three meshes were examined, based on Roache's criteria, r was 2 because the

mesh spacing was halved during each refinement, and p was 2 because a second-order solution method is employed [22]. Grid convergence testing at 88 locations within the vicinity of the patient ($3.25 \leqslant x \leqslant 4.5$, $0.325 \leqslant y \leqslant 0.55$, and $0.9 \leqslant z \leqslant 1.35$) yielded a relative GCI of 5.05×10^{-4}.

Validation of the specific scenario modeled is not provided because no experimental velocity data exist for the case of the health care worker positioned alongside the patient. In fact, Huang and Tsao [12] did not actually validate their grid-independent simulation with their boundary conditions because they did not measure velocity in their experiments. To demonstrate the validity of the code while accounting for the lack of available velocity data for the AIIR, Huang and Tsao [12] simulated a different ventilated room where the air velocity was measured by Chung and Hsu [23] with comparable results. To instill the reader with confidence in the simulations presented here, a simple comparison is provided. Huang and Tsao [12] declared that, for all simulations, velocity was reduced to 0.09 m/s at 0.10 m from the patient's mouth. Fig. 3 shows velocity as a function of distance, d, from the mouth for this simulation. Near the mouth, velocity decreases logarithmically from the mouth as $u = -0.0333\ln(d) + 0.0157$. Velocity is estimated to be 0.092 m/s at a distance of 0.10 m from the mouth based on the modeled data. A comparison is also made for the concentration data. This is presented after the particle simulation description below.

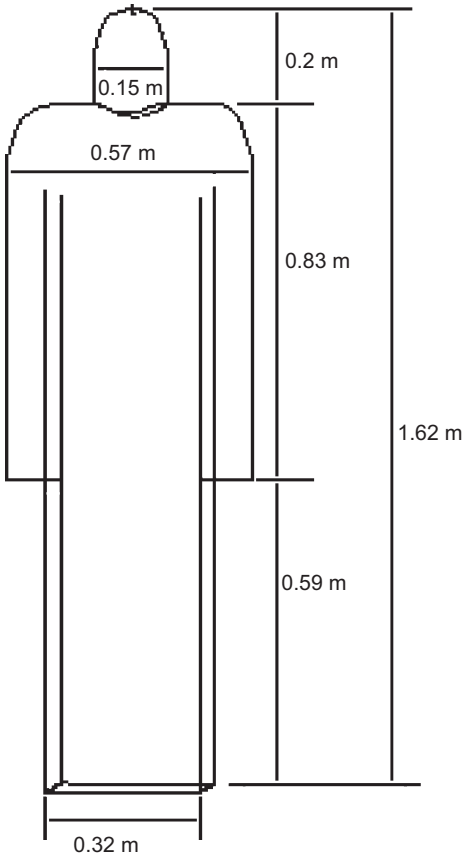

Fig. 2. Geometry of the health care worker.

Lagrangian particle tracking was employed to simulate movement of the pathogen nuclei under the influence of drag:

$$\frac{du_p}{dt} = \frac{1}{\tau}(u - u_p), \tag{2}$$

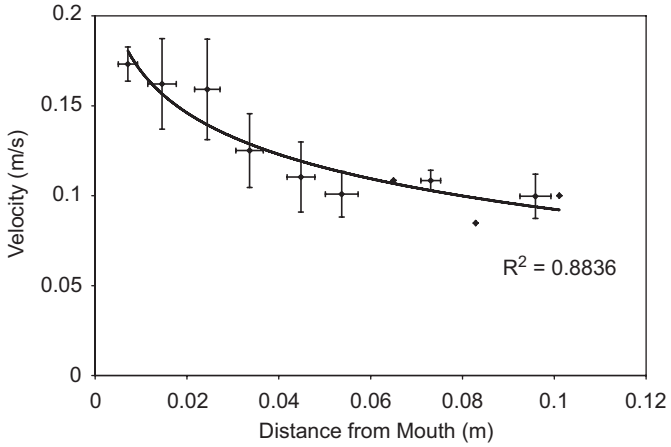

Fig. 3. Air velocity (m/s) just above the patient's mouth vs. distance (m) from the mouth. Error bars in y-direction show standard deviation of velocity, and error bars in x-direction show standard deviation of distance from the mouth.

Table 1
Boundary conditions during CFD simulations

Object	Boundary type	Velocity area (m^2)	Velocity (m/s)	Temperature (K)	TI (%)	Turbulence length scale (m)	Heat generation (w/m^3)
Bed	Wall	–	–	297.15	–	–	0
Door crack	Velocity inlet	0.012	0.694432	295.15	1	0.04375	–
Inlet	Velocity inlet	0.1225	0.612234	295.15	1	0.04375	–
Interior walls	Wall	–	–	297.15	–	–	–
Worker body	Wall	–	–	307.07	–	–	1425
Worker head	Wall	–	–	308.75	–	–	6383
Outer wall	Wall	–	–	303.15	–	–	0
Outlet	Outflow	0.1225	–	–	–	–	–
Patient head	Wall	–	–	311.15	–	–	6383
Patient mouth	Velocity inlet	0.001225	0.2	311.65	1	0.035	–

Note that the breathing boundary condition was maintained even under coughing scenarios, as described in the methods section.

where u_p is the particle velocity, u is the fluid velocity, and τ is particle relaxation time. Because the error in the particle simulation is limited by that of the fluid simulation, the time step size of 0.1 s was used for the particle simulations, as well. The patient was the only source of challenge aerosol representing the pathogenic nuclei, and the aerosol was released at evenly spaced locations over a 0.001225 m^2 opening on the patient's face representing the nose and mouth [12]. The patient lied on his/her back during the simulation to emit the particulate upward. Dry 1 μm particles were used to represent pathogen injected into the room with the saliva evaporated from the particle surface. For the exhalation simulation, 1248 particles were released at a speed of 0.2 m/s during each time step. The simulation was conducted over 90 s, at which time 337,381 particles remained in the domain (some had been removed at the ventilation outlet). For the expulsion simulation, 124,800 particles were released in a single pulse at time = 0 at a speed of 35 m/s. The particle concentration was then allowed to decay in the room over the next 80 s.

To compute concentration, the room (excluding the hallway) was subdivided into 45,540 cubes with dimension 0.1 m × 0.1 m × 0.1 m. Particle number concentration in each cell i, C_i, was computed as:

$$C_i = \frac{n_i}{V_c}, \tag{3}$$

where V_c is the volume of one cell (equal for all cells) and n_i is the number of particles in the ith concentration cell. Number concentration was computed with an in-house FORTRAN95 code that received input from particle trajectory files generated during the FLUENT simulation. Note that this grid was not the same as the tetrahedral mesh used to implement the fluid simulations. This was done for two reasons. First, the irregular tetrahedral grid on which the velocity field was computed would complicate computation of cell volume. Second, cell size was chosen to prevent particles from moving further than one cell within a time step to maintain the Courant requirement $L \geqslant U_{max}\Delta t$, where L = the length of a concentration cube. In this work, $U_{max}\Delta t = (1.08\ m/s)^*(0.05\ s) = 0.054\ m$, which is approximately one-half the cell length. Lastly, concentration was normalized by the flow rate of particles (Q = 12,480 particles/s), the area of the source ($A = 0.001225\ m^2$), and the velocity of particles exiting the mouth (U_0 = 0.2 m/s for breathing or 35 m/s for coughing/sneezing) as

$$\chi = \frac{CU_0}{Q/A}. \tag{4}$$

As discussed above, true validation of the velocity and concentration fields could not be performed because Huang and Tsao's [12] experimental results were not sufficiently discrete to allow for such comparison. Two concentration plumes are presented here for comparison with Huang and Tsao's [12] computational results, which are presented only for the where the ventilation outlet was positioned around (2.5, 3, 2.3). Figs. 4a and 4b display the concentration plume resulting from breathing with the patient lying on its back for this simulation and Huang and Tsao [12], respectively. Here, the shape of the plume is very similar for both simulations. This indicates that the aerosol is pulled towards the ceiling in a similar motion. However, the magnitude of the concentration is approximately an order of magnitude higher for this work. This is likely because the position of the outlet vent for Huang and Tsao [12] pulls the particle-laden air stream away from the wall. Figs. 4c and 4d show the concentration plume resulting from a cough when the patient is lying on his/her side. In this case, the upward motion of the air movement over the patient in this simulation causes the cough plume to rise over the body, whereas the increased motion in the direction of the bed causes more spreading of the plume to the side for Huang and Tsao's [12] simulation. The difference in concentration magnitude is due to the higher velocity of the expulsion for this simulation in comparison with Huang and Tsao's [12], which was 2 m/s. Although these comparisons are not direct, some confidence can be gained given that the differences in the concentration profiles are reasonable given differences in the methodologies used.

3. Results

3.1. Continual breathing

Instantaneous images can be used to track the aerosol plume development. Figs. 5–7 display the plume of aerosol from the patient during breathing at 5, 30, and 90 s after the simulation begins. This series displays the aerosol's affinity to move towards the walls as it approached the ventilation outlet above the patient's head. The majority of aerosol moved directly over the head and into the ventilation outlet. However, some aerosol deviated from that direct trajectory and traveled to either side of the head before ultimately being pulled upwards towards the ventilation outlet. Given that those aerosols' trajectories were not aligned with the ventilation outlet, trapping and recirculation occurred, as seen in Fig. 7.

In Fig. 8, the plume vertical cross-section is shown at the plane at x = 3.75 m, which lay between the patient and the health care worker. In this figure, the concentration field is split into two categories: $\chi \gg 0.1$ and $\chi < 0.1$. Examination reveals that the high concentration region, where χ exceeds 1, was retained within 0.25 m of the wall behind the patient's bed. This portion of the plume was transported directly upward into the vent. This was driven by airflow moving directly upward by the ventilation system, as can be seen from the velocity field along the plane x = 4 m that intersected the mid-section of the patient, shown in Fig. 9. The x = 4 m plane also bisected the ventilation inlet and outlet. From this diagram, it appears that air was effectively circulated from the inlet, along the patient from toe to head, then up to the outlet. Based on the velocity

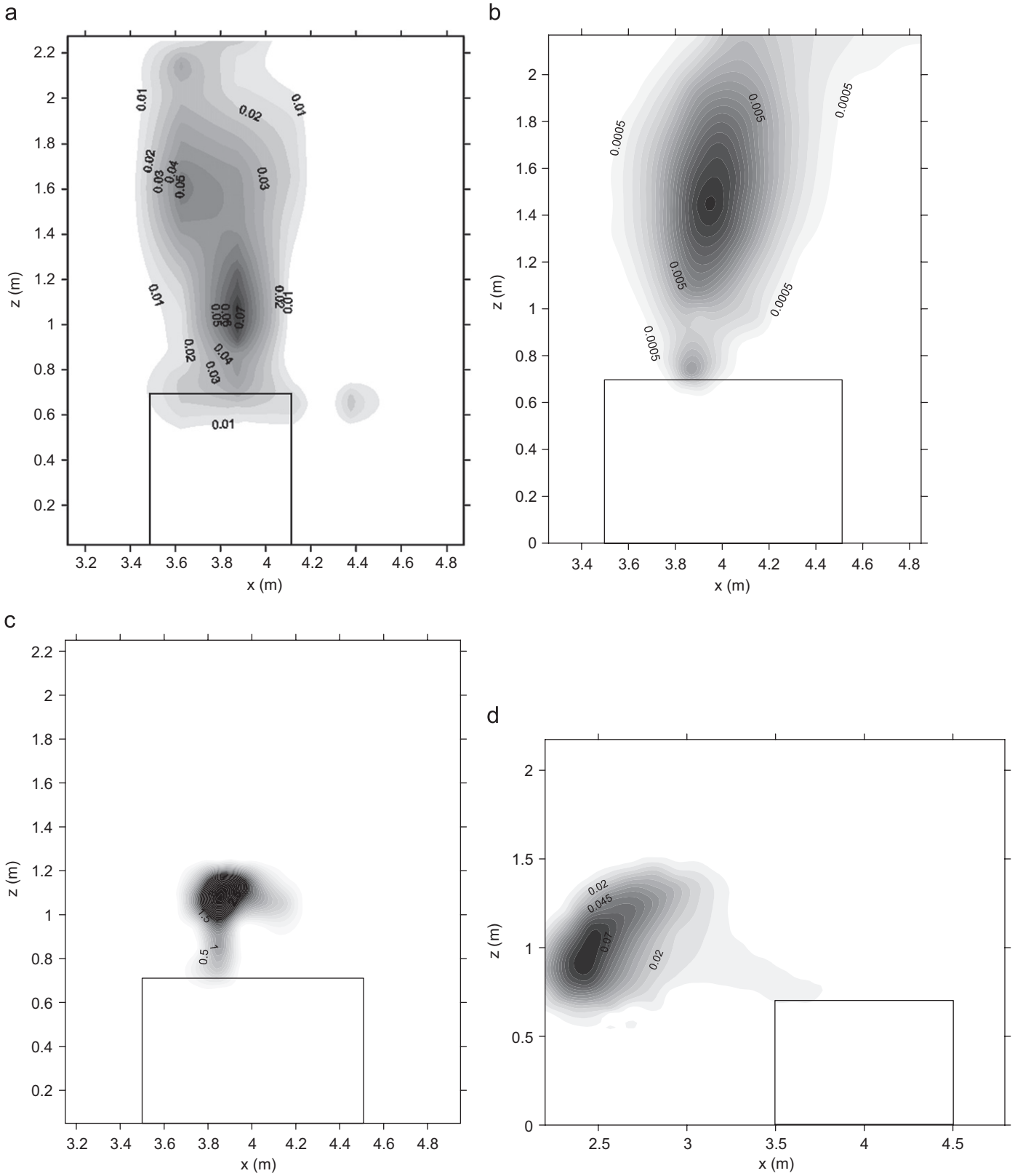

Fig. 4. (a) Time-averaged concentration at $y = 0.05$ during breathing (simulation), (b) time-averaged concentration at $y = 0.05$ during breathing (H&T), (c) concentration at 5 s at $y = 0.05$ after coughing, with the patient lying on the side (simulation), and (d) concentration at 3.5 s at $y = 0.05$ after coughing, with the patient lying on the side (H&T). The patient's bed is outlined for reference. Note that the plume observed below the top of the bed comes behind the patient's head.

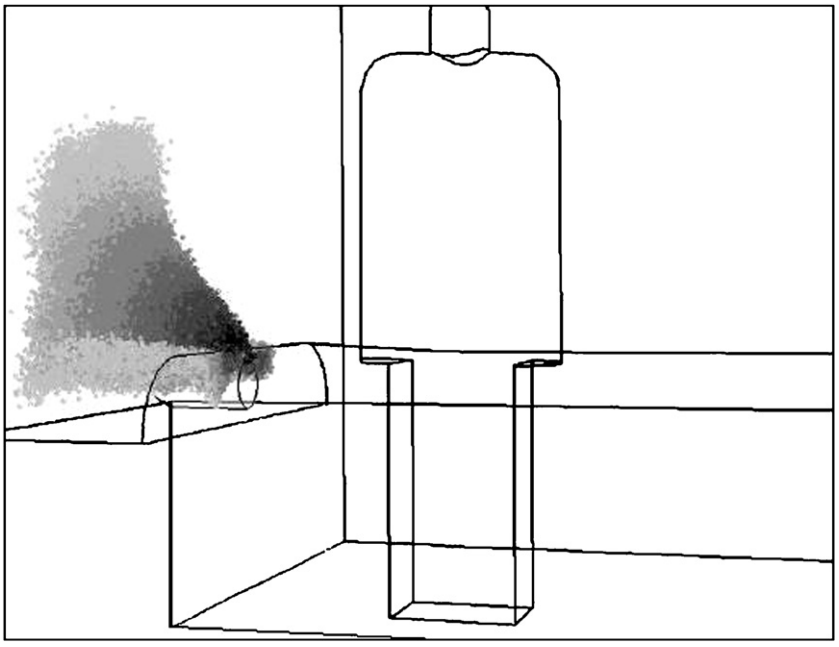

Fig. 5. Aerosol dispersion from continual breathing, 5 s after initial release.

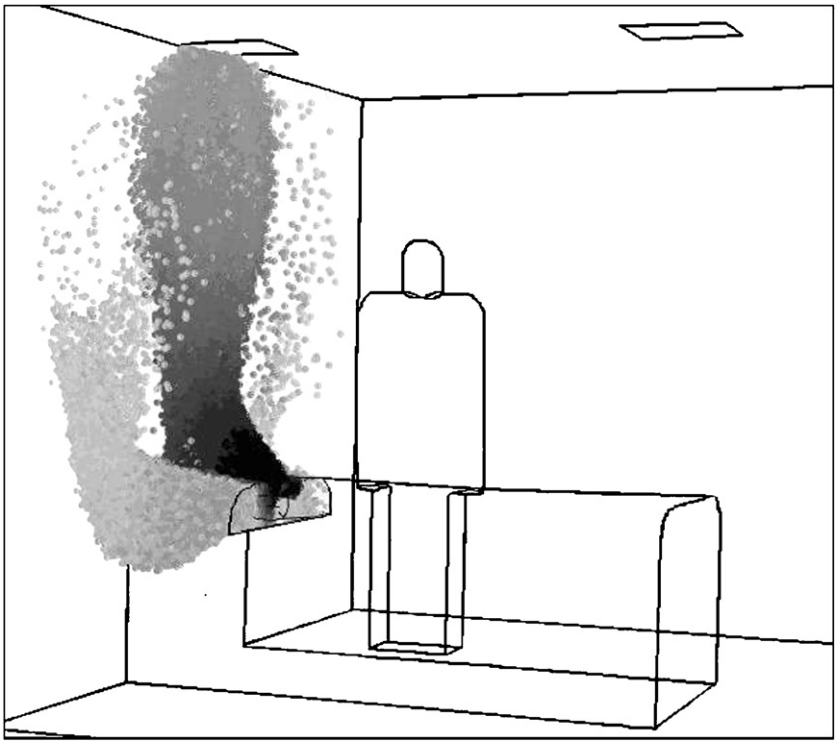

Fig. 6. Aerosol dispersion from continual breathing, 30 s after initial release.

field, the ventilation system appeared to bring fresh air across the health care worker's breathing zone and restrict migration of the contaminant beyond the distance between the patient's breathing zone and the wall.

The airflow and aerosol dispersion patterns varied with distance from the plane $x = 4$ m. Fugitive aerosol in lower concentrations extended beyond the vent along the ceiling, in the region $z > 1.8$ m and $0.25 < y < 1$ m, as shown in Fig. 8. When viewing Fig. 10, which shows the velocity field along the plane $x = 3.3$ m (directly in front of the health care worker's breathing zone), it can be seen that this zone corresponded to a region of recirculatory airflow. Moreover, one additional recirculatory region formed directly in front of the health care worker's face and mid-section, and two others were produced to the right of the health care worker. Figs. 7 and 11 suggest that the aerosol

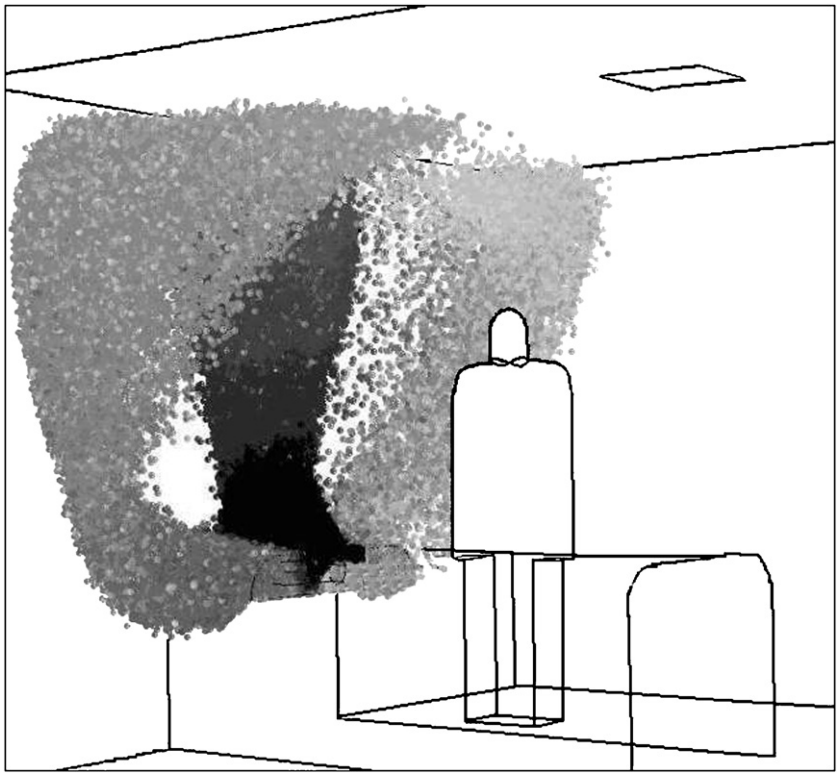

Fig. 7. Aerosol dispersion from continual breathing, 90 s after initial release. To emphasize that the particles have not crossed in front of the health care worker, the worker is represented by a white image where the particles extend behind the worker's back.

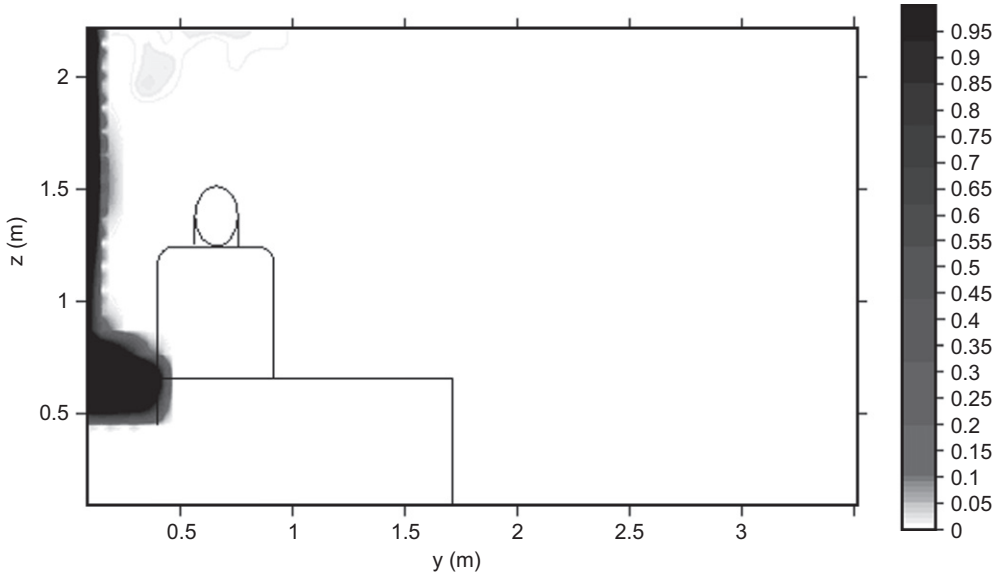

Fig. 8. Cross-section of the plume from continuous breathing after 90 s at $x/L = 3.75$, which intersects the patient bed, outlined for reference.

that was drawn upwards along either side of the bed prior to passing through the region where fugitive aerosols are identified in Fig. 8.

Fig. 11 presents a plan view of aerosol dispersion in the AIIR. In this figure, concentration was integrated from the floor to the ceiling. Three features of the profile are evident. First, the majority of aerosol appears drawn near to the ventilation outlet. Second, the aerosol that deviated from the outlet region tended to move upward and towards the corners of the AIIR, traveling along the back wall of the AIIR before recirculating. Third, based on Figs. 7 and 11 together, the majority of the aerosol that recirculated was located at $z > 1$ m. That tendency of the aerosol to congregate near the wall regions was also observed experimentally by Huang and Tsao [12] for aerosol deposits during a one-hour "breathing" experiment. Results from

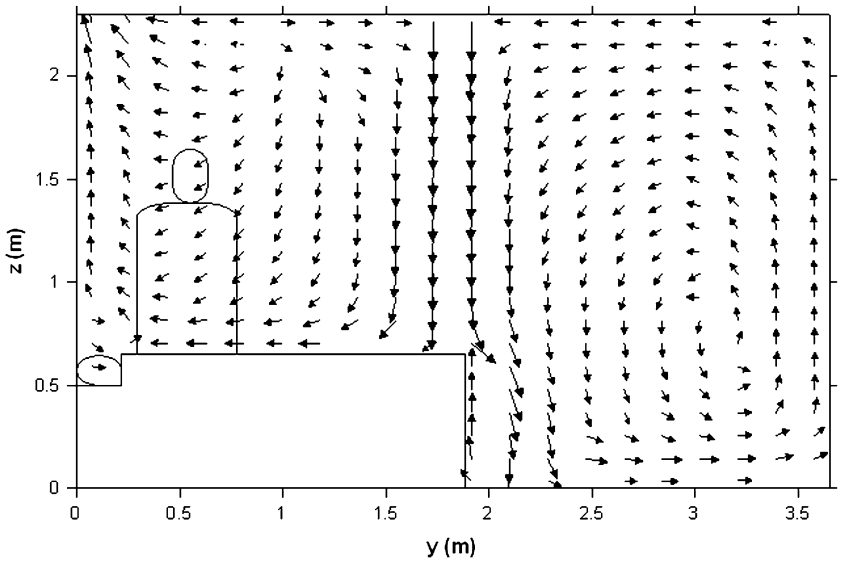

Fig. 9. Velocity profile along the patient cross-section, $x = 4\,\mathrm{m}$.

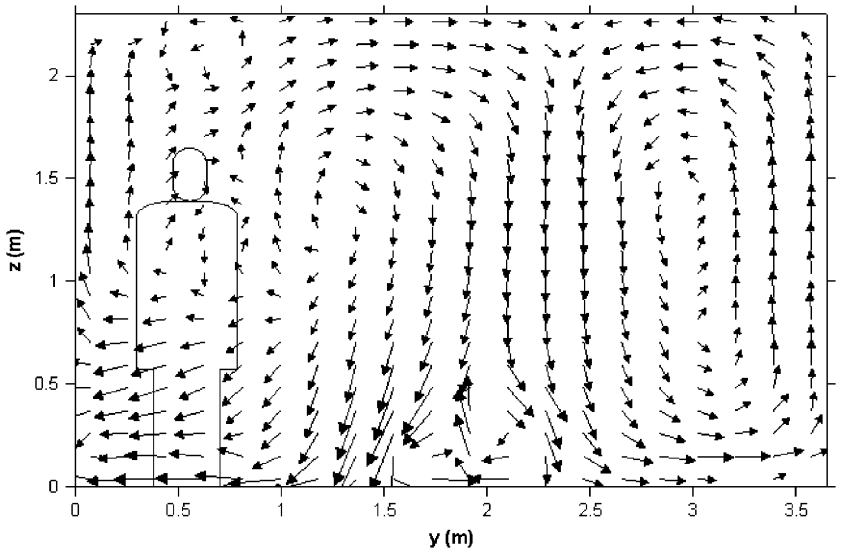

Fig. 10. Velocity profile in front of the health care worker's breathing zone, $x = 3.33\,\mathrm{m}$.

that experiment are mapped in Fig. 12 for the reader's convenience. Although the aerosol deposition profile along the room shows that the aerosols were transported beyond the region near the bed, the majority of deposits were found near the rear and side walls surrounding the bed of the AIIR.

The quantity of aerosol in the nurse's breathing zone was computed to determine how the concentration profile would impact exposure. There are few consistent definitions for breathing zone size and shape in the peer-reviewed literature. Marr et al. [24] characterized the velocity pattern within 4 in. of the face of a heated mannequin. ASHRAE Standard 62-2001 defines the breathing zone as the space of air between 0.7 and 1.8 m from the ground and at least 0.6 m from any side wall [25]. Most personal indoor air sampling studies place sampler inlets at the person's lapel and consider the breathing zone to be the hemisphere in front of the body centered at the mouth. A 0.3 m radius was assumed. With a shoulder-to-shoulder width of 0.57 m and the mouth positioned at (3.3, 0.45, and 1.55), the breathing zone was defined to be the zone in front of the face extending from (3.25, 0.45, and 1.35) through (3.55, 0.85, and 1.85). Within this zone, the concentration is fairly low: $\chi = 2.5 \times 10^{-4}$. This equates to 13 particles entering the health care worker's breathing zone.

3.2. Pulse expulsion (cough/sneeze)

Fig. 13 shows the decay of residual aerosol following the 35 m/s cough/sneeze injection, where the residual is defined as

$$\phi = \frac{\sum_i \chi_i}{\sum_i \chi_{i,0}}, \tag{5}$$

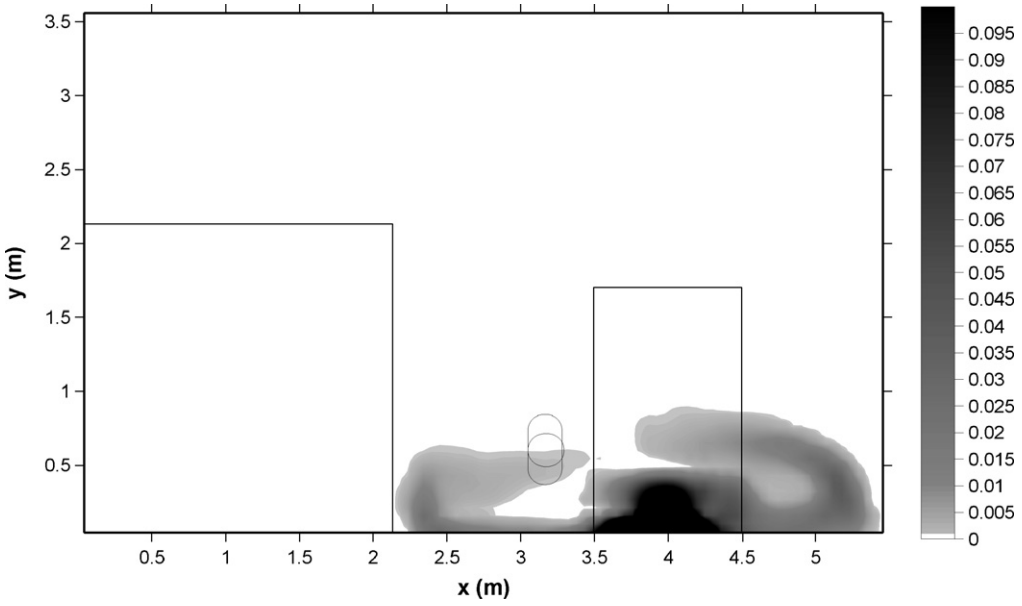

Fig. 11. Plan view of the room after 90 s of continual breathing. Normalized aerosol concentration is integrated over the height of the room. The bathroom, healthcare worker, and bed are outlined for reference. Referring to Fig. 5, much of the suspended aerosol is near the top of the room.

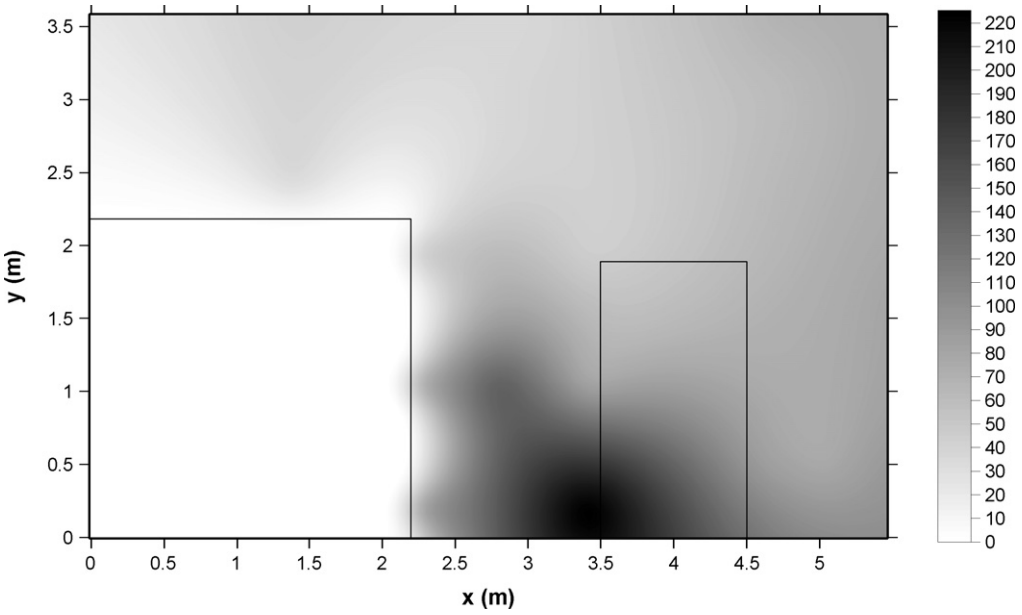

Fig. 12. Plan view of the deposition profile in the room after the Huang and Tsao [12] experiments of continual breathing. The scale represents the number of colony counts at each deposition sample. The bathroom and bed are outlined in this figure (note that no health care worker was included in these experiments). Aerosol settled to the floor in this figure.

where χ is summed over all cells i within the domain and χ_0 indicates the normalized concentration at injection (time = 0 s). Also shown in Fig. 13 is the decay of residual aerosol during the cough modeled by Huang and Tsao [12] with a velocity of 2 m/s.

In both cases, ϕ varied as an inverse function of time. For the 2 m/s cough, derivation of this relationship is straight-forward: $\phi = [3.9934t + 1]^{-1}$. The 35 m/s expulsion modeled in this study shows that aerosol concentrations remain relatively constant over 15 s, at which time ϕ follows an inverse trend: $\phi = 1$, $t < 15$; $\phi = [0.22229(t-15) + 1]^{-1}$, $t \geqslant 15$. In both cases, coincidentally, these curves fit the respective data with $R^2 = 0.94$.

4. Discussion

A number of factors may have been responsible for aerosol dispersion observed in the AIIR model related to the source of aerosol (patient) and airflow characteristics of the room that are driven by ventilation and temperature

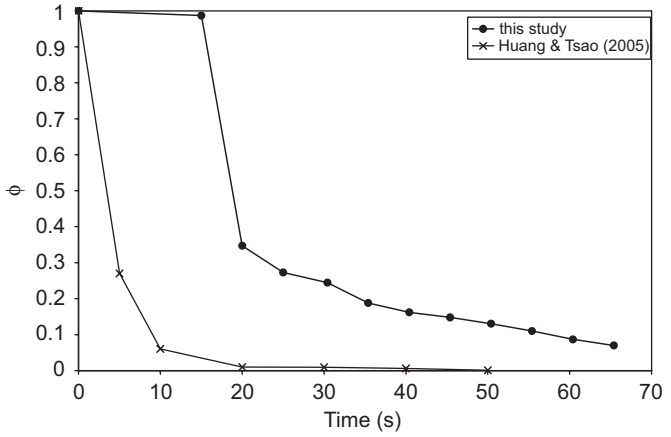

Fig. 13. Residual aerosol after patient has an expulsion (cough/sneeze).

gradients. It is likely that a combination of factors actually led to the presence of fugitive aerosols in the simulation and in the Huang and Tsao [12] experiments.

With respect to the source characteristics, by using an elliptical head shape with a "mouth/nose" fitted to the shape of the head in lieu of a rectangle with a rectangular planar opening, as used in Huang and Tsao [12], the aerosols' initial trajectories varied in direction. Qian et al. [14] illustrated the importance of including a multi-directional source in their experimental work to investigate infectious disease transport in hospital rooms. This directional difference could then have caused the aerosol to exit the mouth as a plume whose spread was more a function of the initial directional differences than of diffusion. The use of a complex shape for the face to produce an initial multi-directional plume is consistent with a study of cough velocity and contaminant concentration in a room with stagnant air [26]. Aerosol on the edges of those plumes could then be swept into recirculating eddies moving along the wall behind the bed. A second reason for initial dispersion of the source plume as it exits the mouth is the presence of a small recirculating region of air just above the patient's head, as can be seen in Fig. 9. Turbulent mixing in this location might also contribute to the lateral spread of aerosols exiting the patient's mouth. In Huang and Tsao [12], this spreading of the source was not observed. However, the use of a square head in their simulation may have removed the multi-directionality of the source and dampened eddy formation directly above the head, the latter of which is observed in a plot of the velocity profile from the Huang and Tsao [12] simulations.

Complexities in the room air velocity profile make turbulence an important factor for the dispersion of the aerosol in the room beyond the source. The majority of aerosol was driven into the outlet vent by the predominant airflow seen in Fig. 9 that swept down along the patient's body and then pulled aerosol up and away from the room occupants. However, the location of fugitive particles shown in Fig. 8 corresponded to the location where a large eddy circulated near the ceiling. It is possible that the length of time for the aerosol to navigate this eddy was extended by the eddy's length because residence time of a pocket of air or particle is inversely proportional to eddy length scale [8,27,28]. This type of large-scale air motion likely delayed mixing and produced gradients of aerosol concentration across the room. Evidence of this was provided by the Huang and Tsao [12] aerosol deposition results. This is an important consideration because, if aerosol should become trapped in the recirculating eddy in front of the health care worker, the potential for exposure could increase appreciably.

An additional factor that may have impacted the particle trajectories less significantly is thermophoresis because the temperature of particles exiting the patient's mouth/nose was 14.5 °C higher than that of the walls behind the bed and next to the bathroom and 8.5 °C higher than the outer wall (at $x = 5.5$ m). It has been shown that warm particles are attracted to cooler surfaces [29]. This affect is likely to help ventilate particles directly above the patient's head, but it also creates the potential for particles released at angles to the mouth/nose to move towards the bathroom and outside walls that surrounded the patient. Thus, thermophoresis may have contributed to the particle spread.

Differences between the residual fraction of aerosol in the 2 and 35 m/s pulse release simulations might also have been related to a number of factors mentioned in this discussion for the case of the breathing patient. For the 35 m/s case, only 1.3% of the particles were exhausted during the first 15 s. More significant reductions proceeded, but at a slower rate than for the 2 m/s exit velocity. Certainly, the difference in exit velocity from the patient should have produced differences in the residual aerosol profile, but it would be expected that the aerosol be exhausted more rapidly for the faster exit speed. The contrary occurred. Again, this may have been driven by multi-directionality of the plume, where the rapid aerosol velocity caused a larger initial dispersion plume. Many particles within that plume had overshot the exhaust vent and concurrently slowed to the speed of the room air. At this point, they encountered slower velocities pulling them towards the exhaust. If carried by air with a velocity of 0.06 m/s (or 10% of the ventilation inlet velocity), particles 1 m away from the exhaust would have required 15 s on average to reach the outlet. Likewise, temporary trapping of aerosols within large eddies could have also produced delays in ventilation.

5. Conclusion

This work illustrated the level of complexity of the airflow and aerosol dispersion patterns within an AIIR under conditions that may, by design, be deemed as favorable for prohibiting the spread of disease. This serves to underscore the importance of understanding mean and turbulent airflow patterns, source dynamics, and other

physical properties of the room and air as causative factors in occupational exposure to airborne contaminants. Future work on this topic needs to focus on the characteristics of large eddies, fine turbulence, room geometry, and source characteristics on dispersion of infectious aerosols and potential exposure to these agents. This research produced limited evidence about the exposure of a health care worker to infectious aerosolized agents in an AIIR. This was largely due to limitations in computational resources that restricted the length of the breathing patient simulation. However, the experimental findings of Huang and Tsao [12], coupled with the slow decay and tendency for particle accumulation near the AIIR walls observed in the simulations presented here, suggests that unintended exposures are possible despite the ventilation system. For this reason, proper functionality of PPE is of utmost importance for protecting health care workers treating infectious disease patients.

Acknowledgment

This research was supported by the NIOSH Universities Occupational Health and Safety Educational Resource Center Pilot Project Training Program, T42-OH008422, administered by the Mt. Sinai-IJ Selikoff Center for Occupational and Environmental Medicine.

References

[1] Yen M-Y, Lin YE, Su I-J, Huang F-Y, Ho M-S, Chang S-C, et al. Using an integrated infection control strategy during outbreak control to minimize nosocomial infection of severe acute respiratory syndrome among healthcare workers. Journal of Hospital Infection 2006;62:195–9.

[2] Fuss EP, Israel E, Baruch N, Roghmann M-C. Improved tuberculosis infection control practices in Maryland acute care hospitals. American Journal of Infection Control 2000;28:133–7.

[3] Centers for Disease Control. Anthropometric reference data, United States, 1988–1994. Accessed 2/5/07 〈http://www.cdc.gov/nchs/about/major/nhanes/Anthropometric%20Measures.htm〉.

[4] Lee K, Slavcev A, Nicas M. Respiratory protection against *Mycobacterium tuberculosis*: quantitative fit test outcomes for five type N95 filtering-facepiece respirators. Journal of Occupational and Environmental Hygiene 2004;1:22–8.

[5] Ofner M, Lem M, Sarwal S, Verancombe M, Simor A. Cluster of severe acute respiratory syndrome cases among protected health-care workers—Toronto, Canada, April 2003. Morbidity and Mortality Weekly Report 2003;52:433–6.

[6] Li Y, Leung GM, Tang JW, Yang X, Chao CYH, Zin JZ, et al. Role of ventilation in airborne transmission of infectious agents in the built environment—a multidisciplinary systematic review. Indoor Air 2007;17:2–18.

[7] Richmond-Bryant J, Eisner AD, Brixey LA, Wiener R. Short-term dispersion of indoor aerosols: can it be assumed the room is well-mixed? Building and Environment 2006;41:156–63.

[8] Richmond-Bryant J, Eisner AD, Brixey LA, Wiener R. Transport of small airborne particles within a room. Indoor Air 2006;16:48–55.

[9] Bjørn E, Nielsen PV. Dispersal of exhaled air and personal exposure in displacement ventilated rooms. Indoor Air 2002;12:147–64.

[10] Qian H, Li Y, Nielsen PV, Hyldgaard CE. Dispersion of exhalation pollutants in a two-bed hospital ward with a downward ventilation system. Building and Environment 2008;43:344–54.

[11] Gadgil AJ, Lobscheid C, Abadie MO, Finlayson EU. Indoor pollutant mixing time in an isothermal closed room: an investigation using CFD. Atmospheric Environment 2003;37:5577–86.

[12] Huang J-M, Tsao S-M. The influence of air motion on bacteria removal in negative pressure isolation rooms. HVAC&R Research 2005;11:563–85.

[13] Cheong KWD, Phua SY. Development of ventilation design strategy for effective removal of pollutant in the isolation room of a hospital. Building and Environment 2006;41:1161–70.

[14] Qian H, Li Y, Nielsen PV, Hyldgaard CE, Wong TW, Chwang ATY. Dispersion of exhaled droplet nuclei in a two-bed hospital ward with three different ventilation systems. Indoor Air 2006;16:111–28.

[15] Alani A, Barton IE, Seymour MJ, Wrobel LC. Application of Lagrangian particle transport model to tuberculosis (TB) bacteria UV dosing in a ventilated isolation room. International Journal of Environmental Health Research 2001;11:219–28.

[16] Shih Y-C, Chiu C-C, Wang O. Dynamic airflow simulation within an isolation room. Building and Environment 2007;42:3194–209.

[17] Launder BE, Spalding DB. The numerical computation of turbulent flows. Computer Methods in Applied Mechanics and Engineering 1974;3:269–89.

[18] Yakhot V, Orszag SA, Thangam S, Gatski TB, Speziale CG. Development of turbulence models for shear flows by a double expansion technique. Physics of Fluids A 1992;4:1510–20.

[19] Shih T, Liou WW, Shabbir A, Yang Z, Zhu J. A new $k\sim e$ eddy viscosity model for high Reynolds number turbulent flows. Computers and Fluids 1995;24:227–38.

[20] Tyaglo IG, Shepelev IA. Dvizhenie vozdushnogo potoha kvytyazhnomu otverstiyu (Airflow near an exhaust opening). Vodosnabzheniei Sanitarnaya Tekhnika 1970;5:24–5 [in Russian].

[21] Betta V, Cascetta F, Labruna P, Palombo A. A numerical approach for air velocity predictions in front of exhaust flanged slot openings. Building and Environment 2004;39:9–18.

[22] Roache PJ. Verification and validation in computational science and engineering. Albuquerque, NM: Hermosa Publishers; 1998.

[23] Chung K-C, Hsu S-P. Effect of ventilation pattern on room air and contaminant distribution. Building and Environment 2001;36:989–98.

[24] Marr D, Khan T, Glauser M, Higuchi H, Zhang J. On particle image velocimetry (PIV) measurements in the breathing zone of a thermal breathing manikin. ASHRAE Transactions 2005;111:299–305.

[25] American Society for Heating, Refrigerating, and Air-Conditioning Engineers. Ventilation for acceptable indoor air quality. ASHRAE 62-2001.

[26] Zhu S, Kato S, Yang J-H. Investigation into airborne transport characteristics of airflow due to coughing in a stagnant indoor environment. ASHRAE Transactions 2006;112:123–33.

[27] Humphries W, Vincent JH. Experiments to investigate transport processes in the near wakes of disks in turbulent air flow. Journal of Fluid Mechanics 1976;75:737–49.

[28] Humphries W, Vincent JH. Near wake properties of axisymmetric bluff body flows. Applied Science Research 1976;32:649–69.

[29] Huang CB, Lin CS. Modeling of aerosol dynamics along a vertical flat plate. Building and Environment 2006;41:568–77.